IEEE Access
Multidisciplinary ⋮ Rapid Review ⋮ Open Access Journal

Received July 28, 2017, accepted August 17, 2017, date of publication August 25, 2017, date of current version September 27, 2017.

Digital Object Identifier 10.1109/ACCESS.2017.2744639

Fault Detection and Location System for Diagnosis of Multiple Faults in Aeroengines

YE YUAN[1], XIAFOENG LIU[2], (Member, IEEE), SHUITING DING[1], AND BOCHAO PAN[1]

[1]School of Energy and Power Engineering, Beijing University of Aeronautics and Astronautics, Beijing 100191, China
[2]School of Transportation Science and Engineering, Beijing University of Aeronautics and Astronautics, Beijing 100191, China

Corresponding author: Xiaofeng Liu (liuxf@buaa.edu.cn)

This work was supported by the National Natural Science Foundation of China under Grant 61573035.

ABSTRACT This paper presents a fault detection and location (FDL) system for the situation of the coexistence of faults and health degradation in aeroengines. The FDL is able to locate the faulty sensors and actuators when the two kinds of faults coexist and avoid the interference of health degradation. The FDL is formed by a matrix of hybrid Kalman filters, and the different performances of hybrid Kalman filters can be used to distinguish the different faults. The proposed approach is applied to the nonlinear aeroengine model, and the ability of the proposed approach to detect and locate the faulty sensors and actuators reliably is demonstrated. According to the results, the FDL is able to locate the faulty sensors and actuators during the interference of health degradation.

INDEX TERMS Kalman filter, aeroengine, onboard model, health degradation, sensor fault, actuator fault.

I. INTRODUCTION

When aeroengines are operated in harsh environments with high temperature, pressure, and speed, the health degradation is unavoidable. The performance of aeroengine components will slowly degrade during regular operations [1], [2]. Unpredictable faults of sensors and actuators may occur during the operation. The failures of sensors, actuators, or components may change the behavior of the aeroengine, and result in the instability of the aeroengine. The faulty sensors will provide incorrect aeroengine output signals for the control system, and the faulty actuators will cause the deviations of the position of actuators, which will cause a mismatch between actual control inputs and the commanded control inputs.

To maintain the stability of aeroengines during the operation, the reliability can be achieved by fault-tolerant control, which utilizes early detection and location of faults. Fault diagnosis is an important part of a fault-tolerant system, and there are various types of tools for fault diagnosis, such as the Kalman filter, fault observers, and neural networks [3]–[7]. The Kalman filter has been demonstrated to be useful in fault diagnosis, and in recent years, a number of diagnostics systems based on the Kalman filter have been developed.

In general, the in-flight fault diagnosis system is designed at a nominal health condition of the aeroengines. This non-degraded condition of aeroengines becomes a reference baseline for the diagnosis system, and the deviations of measured outputs from the reference outputs may be considered to be the presence of a fault. However, the health degradation can cause the outputs of the actual engine to deviate from the reference health baseline. When the mismatch of outputs exceeds a certain level, it becomes difficult to distinguish the faults from the mismatch caused by the health degradation, merely by observing the measured outputs.

Conversely, the number of actuators and sensors are more than the measured outputs of aeroengines, which means that the diagnosis system needs more fault observers or Kalman filters to detect and locate the faults. In actual situations, there are two fault observers: a fault observer for sensors and a fault observer for actuators to accomplish the diagnosis process based on limited measured outputs [8]. However, once the faults of sensors and actuators coexist, the two dependent fault observers will not able to distinguish the two types of faults because the faults will affect the measured outputs of aeroengines jointly.

Currently, the onboard aeroengine model (OBEM) is introduced into the advanced control system, health monitoring, and diagnosis systems to improve the performance and safety of aeroengines. NASA's Glenn Research Center (GRC) has proposed an intelligent engine control system which includes active control, health management, and fault-tolerant control technologies [9], [10]. The latest model-based control system

needs OBEM to compute the unmeasured outputs, such as the aeroengine thrust, compressor stall, and surge [11]. In 2006, the GRC proposed a hybrid structure, which consisted of the Kalman filter and the OBEM, called a hybrid Kalman filter (HKF) [12], [13]. The computed outputs of the OBEM are used as the baseline outputs for fault diagnosis. If a large discrepancy between commanded and true actuator positions exists due to an actuator fault or if there is a mismatch between the signal of sensors and the actual outputs, then deviations of measured outputs between the OBEM and the actual engine can result. The Kalman filter should provide the corresponding estimated results based on the deviations. In past years, the diagnosis algorithm had been used for engine performance estimation and fault diagnosis [14]–[16].

Recently, a real-time self-tuning OBEM was used for health management [17]. Simon *et al.* [17]–[19] presented a real-time self-tuning model for engine performance monitoring and fault diagnostics, which is a hybrid model including OBEM and neural networks. Volponi *et al.* [20], [21] presented an online tuning engine model that is updated by the Kalman filter. Liu *et al.* [22] used a bank of HKFs to identify the functions of sensor fault locations and on-line OBEM tuning. Ding *et al.* [23] instituted an OBEM tuning system developed from hybrid Kalman filters and took advantage of the bank of HKFs and the OBEM tuning system to form a fault-tolerant OBEM tuning structure [24].

In this paper, a fault detection and location (FDL) system that consists of a matrix of HKFs (MHKF) is proposed for the diagnosis of the faults in sensors and actuators during the interference of health degradation. Each HKF in the MHKF can estimate the variations of certain sensor fault and actuator fault, and the FDL will locate the faulty ones based on the performances of the HKFs.

The following contents of this paper include three sections. Section 2 presents the structure of the FDL. Section 3 includes the simulation results, which are used to demonstrate the effectiveness of the FDL. The study's conclusions are discussed in the last section.

II. DESCRIPTION OF FAULT DETECTION AND LOCATION (FDL) SYSTEM

The purpose of the FDL is to locate the coexisting faults based on the variation of measured outputs as quickly as possible. Considering that the coexistence of health degradation and different kinds of faults may occur during the engine operation, the fault diagnosis system should distinguish between the different factors based on limited measured outputs. To solve the problem of coexisting of health degradation and faults, multiple Kalman filters are needed in the diagnosis system.

The FDL is consisted of a matrix of HKFs. The faults of actuators and sensor are modeled by zeroing out a matrix of the state-space matrices of the aeroengines, and each HKF is designated for a certain sensor and actuator. It is noted that when only one actuator or sensor is faulty, this approach will locate the faulty device according to the similar performance of the HKFs at the related row or column. Once a faulty sensor and one faulty actuator coexist, the HKF corresponding to the faulty devices will perform differently from the others. The relationships between the faults and the HKFs in FDL are shown in Fig. 1.

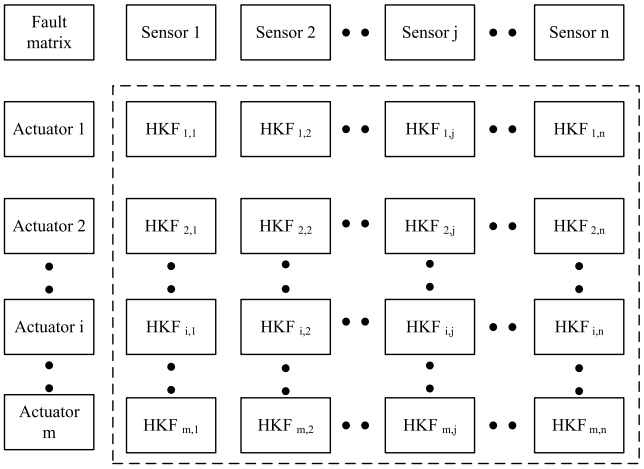

FIGURE 1. Relationship between faults and HKFs.

A. HYBRID KALMAN FILTER (HKF) DESCRIPTION

The structure of an HKF in this paper is shown in Fig. 2. The HKF is a hybrid system consisted of an OBEM and a Kalman filter. In the HKF, the OBEM is used to provide baseline outputs for the Kalman filter. The baseline outputs should not be affected by fault information; therefore, the OBEM should receive control inputs from the actuator models to avoid the influence of faults in actuators. However, considering that the process of health degradation is slow and gradual during one flight mission in general, the OBEM will receive health information off-line to minimize the interference of health degradation [12].

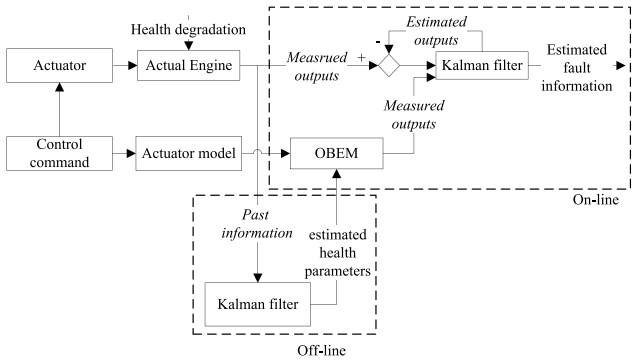

FIGURE 2. Structure of HKF.

The HKF is formulated based on the nonlinear component-level engine model [25]. The model used in this paper is a two-spool high-bypass turbofan engine. Linearization computation is completed based on the two-step perturbation

TABLE 1. Symbol

Symbol	Quantity
f	fault
h	performance degradation factor
u	input parameter
x	state parameter
y	output parameter
z	environmental parameter
DC	degradation coefficient
E	effectiveness
EGT	engine exhaust temperature (k)
EGP	engine exhaust pressure (Pa)
F	flow capacity
N	rotor speed
OT	outlet temperature (k)
OP	outlet pressure (Pa)
W	mass flow
$WSSR$	weighted sum of squared residuals
δ	Scheduled parameter

TABLE 2. Subscript

Subscript	Quantity
kf	Kalman filter
mod	model
ref	reference
ss	steady state
H	high pressure
HPC	high pressure compressor
HPT	high pressure turbine
L	low pressure
LPC	low pressure compressor
LPT	low pressure turbine

method [25]. The linear model is

$$\begin{cases} \Delta\dot{x}(t) = A\Delta x(t) + B\Delta u(t) + L\Delta h(t) + G\Delta z(t) \\ \Delta y(t) = C\Delta x(t) + D\Delta u(t) + M\Delta h(t) + H\Delta z(t) \end{cases} \tag{1}$$

where x represents the state variables of the system, y represents the outputs of the system, u represents the control inputs such as fuel and variable bleeding valve (VBV), h represents the health parameters. The health parameters are the efficiency and flow capacity of the engine compressors and turbines. z represents the environmental inputs such as altitude and Mach number. The operation point of the engine model is used in this paper with the data

$$\begin{aligned} x &= \begin{bmatrix} N_H & N_L \end{bmatrix}^T \\ y &= \begin{bmatrix} N_H & N_L & OT_{fan} & OP_{fan} & OT_{HPC} & OP_{HPC} \end{bmatrix}^T \\ u &= \begin{bmatrix} fuel & VBV \end{bmatrix}^T. \end{aligned}$$

The health parameters are

$$h = \begin{bmatrix} E_{fan} & E_{HPC} & E_{HPT} & E_{LPT} \end{bmatrix}^T.$$

The description of the symbols and subscripts in this paper can be found in Tables I and II.

The model of faults in sensors and actuators can be added in this model for fault diagnosis. An actuator fault is modeled as a bias, which results in an inconsistency between an actuator command received by the OBEM and a true actuator position under which the engine is operating. The bias can be shown by the deviation of control input. A sensor fault is modeled as the mismatch between the signal from a faulty sensor and the corresponding measured output computed by the OBEM. The linear model with both actuator and sensor faults is

$$\begin{cases} \Delta\dot{x}(t) = A\Delta x(t) + B(\Delta u(t) + f_a) + L\Delta h(t) + G\Delta z(t) \\ \Delta y(t) = C\Delta x(t) + D(\Delta u(t) + f_a) + M\Delta h(t) + H\Delta z(t) + Vf_s \end{cases} \tag{2}$$

where f_a is used to represent the bias of control input caused by the actuator fault. f_s is used to show the measurement error of the sensor caused by sensor fault. In this paper, $f_a = \begin{bmatrix} f_{fuel} & f_{VBV} \end{bmatrix}^T$, and $f_s = \begin{bmatrix} f_{N_H} & f_{N_L} & f_{OT_{fan}} & f_{OP_{fan}} & f_{OT_{HPC}} & f_{OP_{HPC}} \end{bmatrix}^T$. To simplify the following description, the actuator faults are marked as $\begin{bmatrix} f_{fuel} & f_{VBV} \end{bmatrix} = \begin{bmatrix} 1 & 2 \end{bmatrix}$ and the sensor faults are marked as $\begin{bmatrix} f_{N_H} & f_{N_L} & f_{OT_{fan}} & f_{OP_{fan}} & f_{OT_{HPC}} & f_{OP_{HPC}} \end{bmatrix} = \begin{bmatrix} 1 & 2 & 3 & 4 & 5 & 6 \end{bmatrix}$. The formula of the Kalman filter can be written as [3]

$$\begin{cases} \Delta\dot{\hat{x}} = A_{kal}\Delta\hat{x} + B\Delta u + L\Delta h + G\Delta z + K_{kal}(y - \hat{y}) \\ \hat{y} = C_{kal}\Delta\hat{x} + D\Delta u + M\Delta h + H\Delta z \end{cases} \tag{3}$$

where

$$\hat{x} = \begin{bmatrix} x \\ h \\ f_a \\ f_s \end{bmatrix}, \quad A_{kal} = \begin{bmatrix} A & L & B & 0 \\ 0 & 0 & 0 & 0 \\ 0 & 0 & 0 & 0 \\ 0 & 0 & 0 & 0 \end{bmatrix}, \quad C_{kal} = [C\ M\ D\ V].$$

As has been described in this paper, each Kalman filter contains faults of an actuator and a sensor, and the state variables of the $HKF_{i,j}$ are $\hat{x} = \begin{bmatrix} N_H & N_L & f_a(i) & f_s(j) \end{bmatrix}^T$. K_{kal} is the gain matrix of Kalman filter, y is the measured output, $\hat{y}$ is the estimated measured output of the Kalman filter. The gain matrix K_{kal} is calculated based on the literature [3].

The form of OBEM in HKF can be described by

$$\begin{cases} \dot{x}_{OBEM} = f(x_{OBEM}, u_{\text{mod}}, h_{ref}, z) \\ y_{OBEM} = g(x_{OBEM}, u_{\text{mod}}, h_{ref}, z) \end{cases} \tag{4}$$

where the OBEM will receive health information h_{ref} during the off-line tuning process. The OBEM is used to provide baseline outputs for the Kalman filter, and the measured outputs of the OBEM can be tuned to adapt to the degraded

engine. The control outputs u_{mod} of the OBEM are provided by corresponding actuators models rather than the signals of actual actuators; therefore, the measured outputs of the OBEM will not be affected by the signal of the faulty actuators. The structure of HKF is simplified because the variations of outputs caused by nominal control inputs, environmental inputs and health parameters are computed by the OBEM. The structure of Kalman filter in HKF is converted into

$$\begin{cases} \Delta\dot{\hat{x}} = A_{kal}\Delta\hat{x} + K_{kal}(y - \hat{y}) \\ \hat{y} = C_{kal}\Delta\hat{x} + y_{OBEM} \end{cases} \tag{5}$$

To adapt to different situations, a linear parameter-varying (LPV) structure is introduced into the HKF. The LPV structure of the HKF is formulated based on the current literature [26]. The nonlinear engine is viewed as a collection of linear models corresponding to the measured outputs and environmental inputs [27]. The LPV model is instituted based on multiple linear models of the operation points. The functions between the elements of the linear models and the scheduling parameters are established, and the scheduling parameters are chosen from the measured outputs of the OBEM and environmental inputs. In the LPV structure, the elements of the matrices will be associated in parallel with the scheduling parameters. In this paper, N_H and environmental inputs are chosen as the scheduling parameters δ in the LPV structure of the HKF. There are functions between the family of scheduling parameters and corresponding elements of matrices in the HKF at different operation points. The elements of the HKF will be tuned in parallel with the variation of δ. Equation (6) and Fig. 3 show the structure of the Kalman filter in HKF

$$\begin{cases} \Delta\dot{\hat{x}} = A_{kal}(\delta)\Delta\hat{x} + K_{kal}(\delta)(y - \hat{y}) \\ \hat{y} = C_{kal}(\delta)\Delta\hat{x} + y_{OBEM}. \end{cases} \tag{6}$$

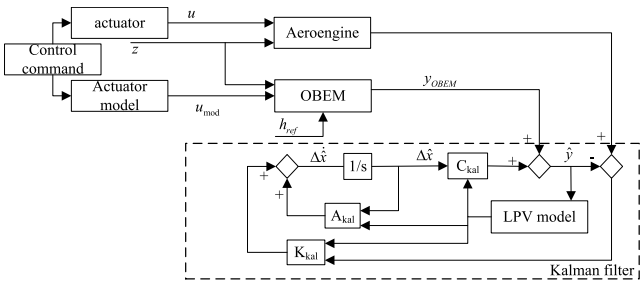

FIGURE 3. Structure of Kalman filter in HKF.

B. MATRIX OF HYBRID KALMAN FILTERS (MHKF)

The number of sensor and actuator faults is more than that of measured outputs of the aeroengine, and the health degradation should be considered during the fault diagnosis process. To solve the coexistence of faults and health degradation, the matrix of HKFs (MHKF) is designed for the FDL to realize the function of detection and location of multiple faults. In the FDL, $m \times n$ HKFs are used, where m is the number of actuators and n is the number of sensors. In addition to the health parameters, each HKF is designated for a corresponding sensor and actuator. The inputs of each HKF are the deviations of n measured outputs between the OBEM and the actual engine.

The fault diagnosis function of the MHKF is carried out based on a weighted sum of squared residuals($WSSR$) [1]. There are two kinds of $WSSR$ for the HKF, one is the $WSSR_{HKF}$, which represents the deviation of outputs between the HKF and actual engine. The other $WSSR$ is $WSSR_{OBEM}$, which represents the deviation of outputs between the OBEM and actual engine. The fault location function is formulated based on the $WSSR_{HKF}s$. The formula for $WSSR$ is

$$\begin{cases} WSSR_{HKF}^{i,j} = W_r(e_{HKF}^{i,j})^T e_{HKF}^{i,j} \\ WSSR_{OBEM} = W_r(e_{OBEM})^T e_{OBEM} \end{cases} \tag{7}$$

where $e_{HKF}^{i,j} = y - \hat{y}^{i,j}$, $e_{OBEM} = y - y_{OBEM}$, and y are the measured outputs from sensors. y_{OBEM} are the corresponding outputs from the OBEM used as the baseline outputs for the HKFs, and $\hat{y}^{i,j}$ are the corresponding estimated outputs of the $\text{HKF}_{\text{i,j}}$, and W_r^i represent the weighting factor, $W_r^i = (y_{OBEM})^{-2}$. For example, the $WSSR_{HKF}^{1,1}$ is computed by the HKF corresponding to f_{fuel} and f_{N_H}. The $WSSR$ in this paper is non-dimensional. The computation of $WSSR_{HKF}s$ are shown in Fig. 4.

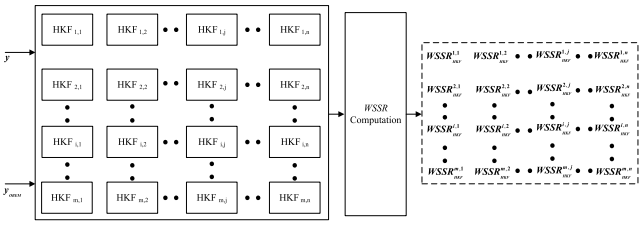

FIGURE 4. Computation of $WSSR_{HKF}$.

The fault diagnosis logics are designed based on the differences of $WSSR_{HKF}s$ of MHKF. If there is no fault, all $WSSR_{HKF}s$ are lower than the corresponding thresholds and diagnostics result of MHKF will show that there is no faulty sensor or actuator. If *ith* actuator is faulty, the $WSSR_{HKF}s$ of the HKF in *ith* row corresponding to the faulty actuator will be lower than the corresponding thresholds, and the remaining $WSSR_{HKF}s$ of $m - 1$ rows are higher than the thresholds. Therefore, the faulty actuator can be located. The location logics of the faulty sensor and the coexisting faults are similar with that of the faulty actuator. The fault location logics are shown in Fig. 5.

There are $m \times n$ thresholds $\lambda_{(m,n)}$ in diagnosis logic, and each $\lambda_{(i,j)}$ is set for the corresponding HKF. Setting the threshold $\lambda_{(i,j)}$ at a low value increases the chance of detecting faults but also increases the chance of generating false alarms. It is reasonable to use different threshold values at different power settings to achieve an effective fault detection performance. The setting of thresholds has been discussed in the literature [12]. The sensors have measurement deviations,

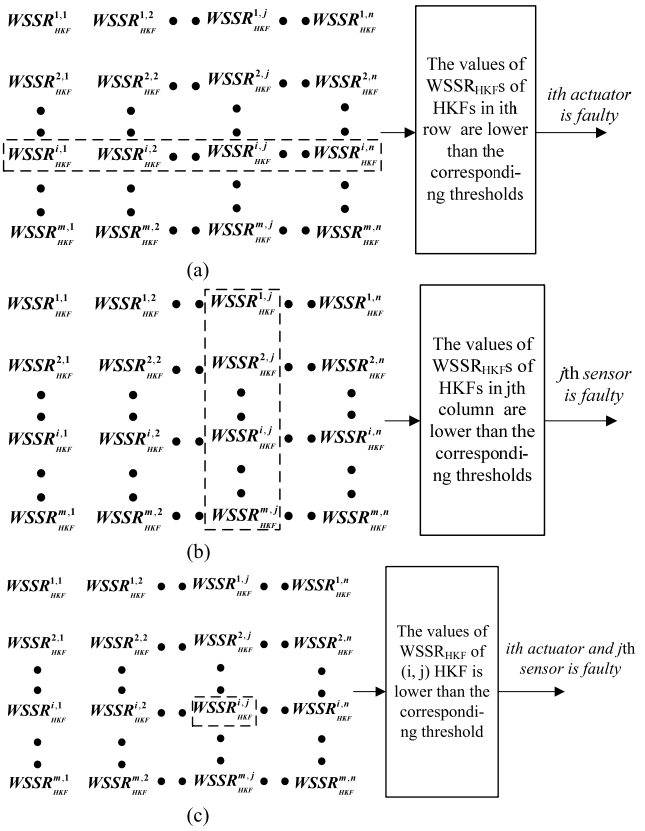

FIGURE 5. **Fault location logics. (a) Actuator fault location logic. (b) Sensor fault location logic. (c) Location logic for coexisting faults.**

and the mismatch caused by the deviations of sensors is unavoidable. Thus, the standard deviations of sensors should be considered in the selection of thresholds. In this paper, *WSSRs* have been computed with a dimensionless treatment; thus, the thresholds of different HKFs should be set at the same order of magnitude at the same power setting.

III. SIMULATION RESULTS

Considering that the length of this paper is limited, as an example, the data of only one operation point is shown in this paper. To show the variations in health parameters directly, the degradation coefficients (*DCs*) of the health parameters are used to represent the ratio of the degraded health parameters to the nominal health parameter. In the model, the *DCs* of the health parameters are defined as

$$\begin{cases} DC_{E_{fan}} = E_{fan,\deg radation}/E_{fan,noimal} \\ DC_{E_{HPC}} = E_{HPC,\deg radation}/E_{HPC,noimal} \\ DC_{E_{HPT}} = E_{HPT,\deg radation}/E_{HPT,noimal} \\ DC_{E_{LPT}} = E_{LPT,\deg radation}/E_{LPT,noimal}. \end{cases} \tag{8}$$

One static-state point is $x = \begin{bmatrix} 8195 & 4890 \end{bmatrix}^T$, and the corresponding matrices are

$$A = \begin{bmatrix} -1.2367 & -0.9043 \\ 0.4389 & -0.9788 \end{bmatrix},$$

$$B = \begin{bmatrix} 9.4273e3 & 1.9668 \\ 2.8613e3 & -1.3856 \end{bmatrix},$$

$$C = \begin{bmatrix} 1 & 0 \\ 0 & 1 \\ -2.2447e\text{-}4 & 8.78156e\text{-}3 \\ -0.3821 & 11.9042 \\ -2.9589e\text{-}2 & -8.7041e\text{-}2 \\ 3.5740 & 5.9852 \end{bmatrix},$$

$$D = \begin{bmatrix} 0 & 0 \\ 0 & 0 \\ 8.6426e\text{-}2 & -6.3962e\text{-}4 \\ 1.4095e2 & -1.0873 \\ 7.5527e2 & 0.1931 \\ 2.1246e4 & -1.6412e1 \end{bmatrix},$$

$$L = \begin{bmatrix} 3.2868e2 & -9.7321e3 & -1.3507e4 & -3.3982e1 \\ -3.3027e3 & 8.4198e2 & 1.0114e3 & -3.5716e3 \end{bmatrix},$$

$$M = \begin{bmatrix} 0 & 0 & 0 & 0 \\ 0 & 0 & 0 & 0 \\ 2.6656e1 & 6.68320e\text{-}2 & 5.7655e\text{-}2 & 3.6176e\text{-}2 \\ 1.5106e3 & 1.1405e2 & 9.9133e1 & 7.0065e1 \\ 6.6511e1 & 2.4102e2 & 2.6755e2 & 2.0250e2 \\ -2.1483e3 & 6.1995e3 & 7.5072e3 & 5.8975e3 \end{bmatrix}.$$

The first simulation shows how the FDL locates the faulty sensor based on $WSSR_{HKF}s$ and when the faulty sensor and health degradation coexist. In the simulation, the engine is working under a static-state condition, and at t = 1 s the sensor of N_L is faulty, which means there is a mismatch between the actual value and the sensor output. The effectiveness of the fan and the HPC was decreased by 1%, which will cause the mismatch between the OBEM and the actual engine. The FDL should locate the faulty sensor during the interference of health degradation. The estimated results of HKFs are shown in Fig. 6.

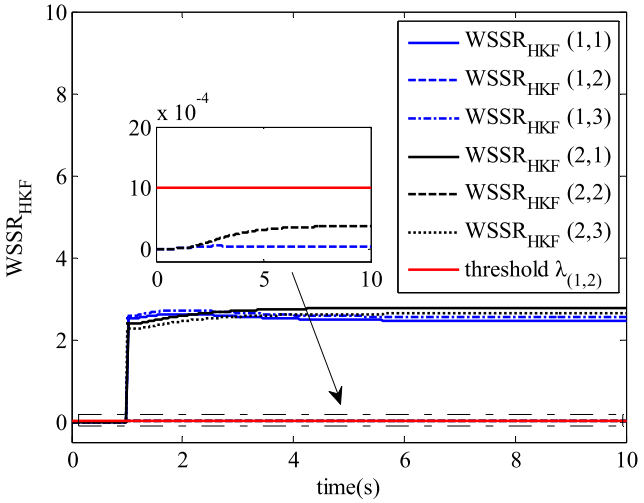

FIGURE 6. ***WSSR$_{HKF}$s* of different HKFs.**

There are six $WSSR_{HKF}s$ and one threshold $\lambda_{(1,2)}$ in Fig. 6. The thresholds $\lambda_{(m,n)}$ are set at the same order of magnitude.

The $WSSR_{HKF}s$ of $HKF_{1,2}$ and $HKF_{2,2}$ corresponding to the sensor of N_L are lower than their corresponding thresholds, and the other $WSSR_{HKF}s$ are higher than the thresholds. According to the differences between the $WSSR_{HKF}s$, the senor of N_L is faulty and the corresponding signal is false.

The thresholds $\lambda_{(m,n)}$ are selected based on the standard deviations of the sensors. In this paper, the thresholds $\lambda_{(m,n)}$ are set as the squared sum of standard deviations to avoid a false diagnosis result. According to the standard deviations of different sensors in the literature [16], the thresholds can be computed.

The second simulation demonstrates how the FDL locates the faulty actuator based on $WSSR_{HKF}s$ when the faulty actuator and health degradation coexist. In the simulation, at t = 1 s the fuel input decreases from 0.4 kg/s to 0.36 kg/s because of fault, and the effectiveness of the fan and the HPC decrease by 1%. The FDL should locate the faulty actuator during the influence of health degradation. The performances of the HKFs are shown in Fig. 7.

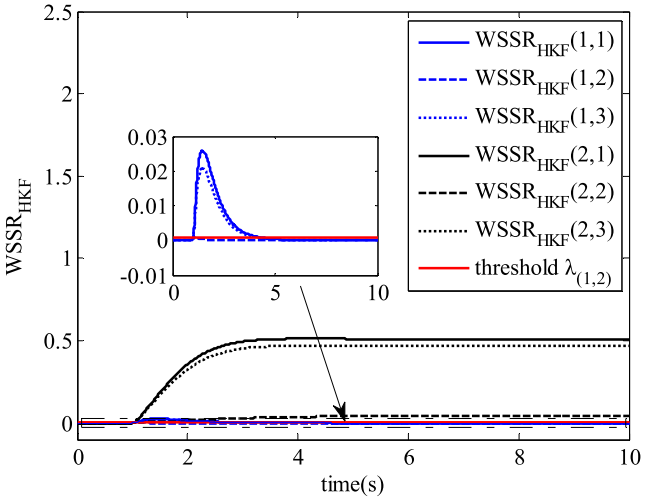

FIGURE 7. $WSSR_{HKF}s$ of different HKFs.

The $WSSR_{HKF}s$ of $HKF_{1,1}$, $HKF_{1,2}$ and $HKF_{1,3}$ corresponding to fuel are all lower than the related thresholds, and the other $WSSR_{HKF}s$ are higher than the thresholds. Based on the performances of $WSSR_{HKF}s$, the faulty actuator is located.

The last simulation is used to demonstrate the effectiveness of the FDL when the faulty sensor, faulty actuator, and health degradation coexist. In the simulation at t = 1 s the fuel input decreases because of fault, the sensor of N_L is faulty, and the effectiveness of the fan and the HPC both decrease. The FDL should distinguish the faulty actuator and faulty sensor according to the deviations of measured outputs. The estimated results of MHKF are shown in Fig. 8.

The $WSSR_{HKF}s$ of $HKF_{1,2}$ corresponding to the actuator of fuel and sensor of N_L is lower than the threshold $\lambda_{(1,2)}$, and the other $WSSR_{HKF}s$ are higher than the related thresholds, which means the senor of N_L and the actuator of fuel are both faulty.

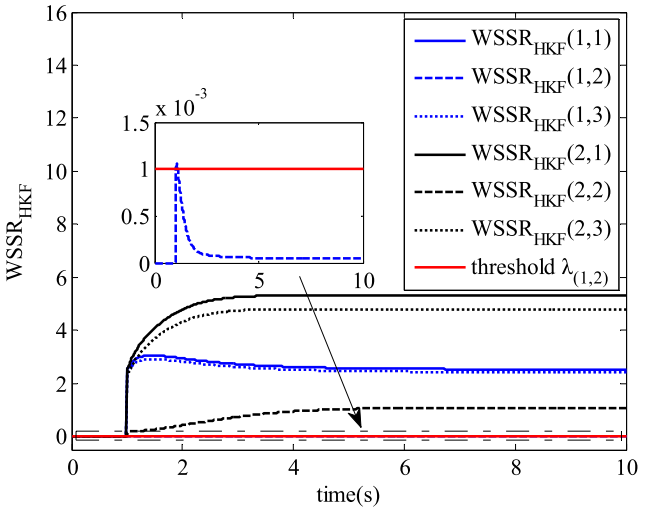

FIGURE 8. $WSSR_{HKF}s$ of different HKFs.

IV. CONCLUSIONS

A fault detection and location system has been represented for the situation of the coexistence of fault and health degradation in aeroengines during their operation. In this system, a matrix of HKFs was used to locate the faulty sensors and actuators based on the different performances of the HKFs. In the HKF, the OBEM received control inputs from the actuator models to avoid the influence of signals from faulty actuators, and off-line health information is provided for the OBEM to minimize mismatching measured outputs due to health degradation. The simulation results have demonstrated that this system can distinguish faulty actuators and faulty sensors during the interference of health degradation and can locate the faulty ones.

REFERENCES

[1] A. Jeffrey and D. Simon, "Implementation of an integrated on-board aircraft engine diagnostic architecture," in *Proc. AIAA/ASME/SAE/ASEE Joint Propuls. Conf. Exhib.*, 2012, pp. 1–5.

[2] K. Takahisa and D. L. Simon, "Integration of on-line and off-line diagnostic algorithms for aircraft engine health management," *J. Eng. Gas Turbines Power*, vol. 129, no. 4, pp. 649–659, 2007.

[3] D. L. Simon and S. Garg. (2003). "Aircraft engine sensor/actuator/component fault diagnosis using a bank of Kalman filters," NASA Glenn Res. Center, Cleveland, OH, USA, Tech. Rep. NASA/CR-2003-212298, NAS 1.26:212298, E-13862. [Online]. Available: https://ntrs.nasa.gov/search.jsp?R=20030032975

[4] J. Chen, J. R. Patton, and G.-P. Liu, "Optimal residual design for fault diagnosis using multi-objective optimization and genetic algorithms," *Int. J. Syst. Sci.*, vol. 27, no. 6, p. 567, 1996.

[5] H. Wang and S. Daley, "Actuator fault diagnosis: An adaptive observer-based technique," *IEEE Trans. Autom. Control*, vol. 41, no. 7, pp. 1073–1078, Jul. 1996.

[6] K. K. Botros, G. Kibrya, and A. Glover, "A demonstration of artificial neural-networks-based data mining for gas-turbine-driven compressor station," *J. Mol. Biol.*, vol. 389, no. 1, pp. 58–73, 2002.

[7] M. R. Napolitano, D. A. Windon, J. L. Casanova, M. Innocenti, and G. Silvestri, "Kalman filters and neural-network schemes for sensor validation in flight control systems," *IEEE Trans. Control Syst. Technol.*, vol. 6, no. 5, pp. 596–611, Sep. 1998.

[8] S. Montadher and R. J. Patton, "Active fault tolerant control for nonlinear systems with simultaneous actuator and sensor faults," *Int. J. Control Autom. Syst.*, vol. 11, no. 6, pp. 1149–1161, 2013.

[9] S. Garg, "Controls and health management technologies for intelligent aerospace propulsion systems," in *Proc. Aerosp. Sci. Meet. Exhib. (AIAA)*, 2004, pp. 5–28.
[10] J. S. Litt *et al.*, "A survey of intelligent control and health management technologies for aircraft propulsion systems," *J. Aerosp. Comput. Inf. Commun.*, vol. 1, no. 12, pp. 543–563, Dec. 2005.
[11] B. Alireza, S. Adibhatla, and C. Rauche, "Integrated model-based controls and PHM for improving turbine engine performance, reliability, and cost," in *Proc. 45th AIAA/ASME/SAE/ASEE Joint Propuls. Conf. Exhib.*, 2013, pp. 1–5.
[12] K. Takahisa and D. L. Simon. (2006). "Hybrid Kalman filter: A new approach for aircraft engine in-flight diagnostics," NASA, Cleveland, OH, USA, Tech. Rep. NASA/TM-2006-214491, E-15783, ARL-TR-4001. [Online]. Available: https://ntrs.nasa.gov/search.jsp?R=20070002904
[13] K. Takahisa and D. L. Simon, "Hybrid Kalman filter approach for aircraft engine in-flight diagnostics: Sensor fault detection case," *J. Eng. Gas Turbines Power*, vol. 129, no. 3, pp. 745–755, 2007.
[14] S. Garg, "Propulsion controls and diagnostics research at NASA Glenn," in *Proc. 43rd AIAA/ASME/SAE/ASEE Joint Propul. Conf. Exhibit*, 2007. [Online]. Available: https://arc.aiaa.org/doi/abs/10.2514/6.2007-5713
[15] S. Donald and S. Garg, "A systematic approach for model-based aircraft engine performance estimation," in *Proc. AIAA Infotech Aerosp. Conf.*, 2013. [Online]. Available: https://ntrs.nasa.gov/search.jsp?R=20100006915
[16] B. Pourbabaee, N. Meskin, and K. Khorasani, "Multiple-model based sensor fault diagnosis using hybrid Kalman filter approach for nonlinear gas turbine engines," in *Proc. Amer. Control Conf.*, Jun. 2013, p. 4717.
[17] J. B. Armstrong and D. L. Simon, "Constructing an efficient self-tuning aircraft engine model for control and health management applications," in *Proc. Annu. Conf. Prognostics Health Manage. Soc.*, 2012, pp. 1–12.
[18] D. L. Simon and J. B. Armstrong, "An integrated approach for aircraft engine performance estimation and fault diagnostics," in *Proc. Turbo Expo Turbine Tech. Conf. Expo.*, 2012, p. 935.
[19] "An integrated architecture for aircraft engine performance monitoring and fault diagnostics: Engine test results," in *Proc. AIAA/ASME/SAE/ASEE Joint Propuls. Conf.*, 2015, pp. 1–5.
[20] A. Volponi, "Enhanced self tuning on-board real-time model (eSTORM) for aircraft engine performance health tracking," Pratt Whitney Aircraft, East Hartford, CT, USA, Tech. Rep. FR-26751, 2008.
[21] A. Volponi, T. Brotherton, and R. Luppold, "Empirical tuning of an on-board gas turbine engine model for real-time module performance estimation," *J. Eng. Gas Turbines Power*, vol. 130, no. 2, pp. 669–678, 2007.
[22] X. Liu, N. Xue, and Y. Yuan, "Aircraft engine sensor fault diagnostics using an on-line OBEM update method," *PLoS One*, vol. 12, no. 2, p. e0171037, 2017.
[23] D. Shuiting, Y. Yuan, N. Xue, and X. Liu, "An onboard aeroengine model-tuning system," *J. Aerosp. Eng.*, vol. 30, no. 4, 2017. [Online]. Available: http://ascelibrary.org/doi/abs/10.1061/%28ASCE%29AS.1943-5525.0000726
[24] D. Shuiting, Y. Yuan, N. Xue, and X. Liu, "Online fault-tolerant onboard aeroengine model tuning structure," *Int. J. Aerosp. Eng.*, vol. 2016, no. 12, pp. 1–15, 2016. [Online]. Available: https://www.hindawi.com/journals/ijae/2016/7904657/
[25] J. C. Link and J. D. Mattingly, *Aircraft Engine Controls : Design, System Analysis, and Health Monitoring*. Washington, DC, USA: AIAA, 2009.
[26] L. Reberga and D. Henrion, "LPV modeling of a turbofan engine," in *Proc. IFAC*, vol. 38, no. 1, pp. 526–531, 2005.
[27] T. Roland, *Modeling and Identification of Linear Parameter-Varying Systems*. (Lecture Notes in Control & Information Sciences), vol. 403. Reston, VA, USA: Amer. Soc. Civil Eng., 2010.

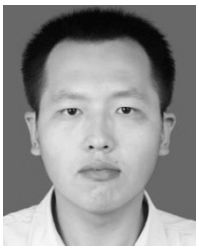

YE YUAN received the B.S. degree in electrical engineering and automation from the Civil Aviation University of China, Tianjin, China, in 2009, and the M.S. degree in transportation engineering from the Beijing University of Aeronautics and Astronautics, Beijing, China, in 2013. He is currently pursuing the Ph.D. degree at the School of Energy and Power Engineering, Beihang University, Beijing. His main research interest is fault-tolerant control of aircraft engines.

XIAFOENG LIU (M'16) received the B.S., M.S., and Ph.D. degrees in power machinery engineering from the Harbin Institute of Technology, Harbin, China, in 2002, 2004, and 2008, respectively. His main research interests are dynamic modeling and control of aircraft engines. He is currently an Associate Professor and an M.S. Supervisor with the School of Transportation Science and Engineering, Beihang University, Beijing, China. His main research interests, including aircraft engine modeling, control and degradation/fault on-line diagnostics and estimation.

SHUITING DING received the B.S. degree in thermal power engineering from the Beijing University of Aeronautics and Astronautics, Beijing, China, in 1990, and the M.S. and Ph.D. degrees in propulsion theory and engineering from the Beijing University of Aeronautics and Astronautics, Beijing, in 1993 and1998, respectively.

He is currently a Professor and a Doctoral Supervisor and the Dean of the School of Energy and Power Engineering, Beihang University, Beijing. He is an Academic Leader of the innovative project Safety of Aircraft Engine in MOE, the Director and a Chief Scientist with the Innovation Center of Advance Aircraft Engine of MOE, in 2011. He has authored over 60 papers in safety and airworthiness of aircraft engines. He holds over 20 patents. He was the recipient of the National Award for Technological Invention.

BOCHAO PAN was born in 1991. He received the B.S. degree in flight vehicle propulsion engineering from Beihang University, Beijing, China, in 2013. He is currently pursuing the master's degree at the College of Energy and Power Engineering, Beijing University of Aeronautics and Astronautics. His main research interest is safety of aircraft engines.